ELSEVIER

Polymer 40 (1999) 4635–4646

polymer

# Molecular structure and orientation in processed polymers 1. Analysis of X-ray scattering data

D.C. Oda, G.C. Rutledge*

*Department of Chemical Engineering, Massachusetts Institute of Technology, Cambridge, MA 02139, USA*

Dedicated to Professor Ronald K. Eby on the occasion of his 70th birthday

Received 12 September 1998; received in revised form 23 December 1998; accepted 28 December 1998

**Abstract**

We present a method for analyzing the molecular scale orientation and structure of processed polymers using wide angle X-ray scattering data (WAXS). The technique is applied to the analysis of solution-spun fibers of a liquid crystalline polyester comprised of 1,4-hydroxybenzoic acid, isophthalic acid, and hydroquinone. The orientation distribution function (ODF) of the non-crystalline component of the polyester is constructed using a Legendre polynomial series expansion. To construct a consistent molecular scale description, a Monte Carlo sampling scheme which incorporates the standard Metropolis sampling was employed, coupled with a weighting factor that favors structures which are in closer accord with the experimental WAXS data. The members of the ensemble sampled by the simulation consist of rhombic lattices on which oligomers are placed in an aligned state. The conformation of each oligomer was obtained using a rotational isomeric state description. By direct comparison of the experimental and calculated structure factor coefficients, the ODF for the structural ensemble was deduced. For the polyester fiber considered here, a two-component system consisting of oriented and unoriented non-crystalline components is required for complete characterization of the scattering properties of the sample. The sample contains a negligible amount of crystalline material, but 85% of the sample is aligned locally (i.e. with respect to nearest neighbor chains). However, as the fibers are spun from an isotropic solution, the global orientation (i.e. orientation with respect to the sample axis) remains low. 

*Keywords:* Wide angle X-ray scattering; Orientation distribution function; Molecular simulations

## 1. Introduction

Post-synthesis processing of polymers has a huge impact on the bulk properties, such as tensile strength and modulus, observed in engineering materials. In many cases, the morphology is altered all the way down to the molecular scale. This is generally true of polymers, and is especially important in cases such as fiber spinning, where very high process rates and flow stresses induce large changes in the morphology of the final product on all length scales. One class of polymers where molecular orientation is known to have a predominant role in determining properties is liquid crystal polymers (LCPs), which are used for high strength, high modulus applications. These include lyotropic LCPs, such as the aramids Kevlar[tm] and Nomex[tm], and thermotropic LCPs such as Vectra[tm] and related copolyesters. In this work, we focus our attention on a class of copolyesters composed of $x$ mol% 1,4-hydroxybenzoic acid (H) and $(100 - x)/2$ mol% each of isophthalic acid (I) and hydroquinone (Q), which we denote as HIQ-$x$. This copolyester is thermotropic in the range $20 < x < 80$; between $20 < x < 50$, liquid crystallinity is exhibited within a window of about 50°C [1,2]. It is also soluble in a mixed solvent of dichloromethane and trifluoroacetic acid [3].

HIQ-$x$ has been studied fairly extensively by wide angle X-ray scattering (WAXS) [1,2,4–6] for the purpose of determining crystallinity and crystal structure. WAXS is also useful for analyzing the orientation distribution of the crystalline component in highly oriented melt-spun fibers. To date, X-ray analysis on HIQ-$x$ has focused on elucidating the unit cell structure of HIQ-33 and HIQ-50 fibers [1,2,4]. For the HIQ family of polymers, Erdemir et al. proposed an orthorhombic fiber unit cell with $a = 5.58$ Å, $b = 3.92$ Å, and $c = 24.32$ Å ($\rho = 1.49$ g/cm$^3$) [5]. A similar unit cell was reported by Blundell [1]. The HIQ-$x$ powder unit cell ($20 < x < 80$) was shown experimentally to be very similar to that of poly($p$-phenylene isophthalate) (HIQ-0) [2,7]. O'Mahoney et al. investigated single crystals of model

* Corresponding author. Tel.: + 1-617-253-0171; fax: + 1-617-258-0546.

*E-mail address:* rutledge@mit.edu (G.C. Rutledge)

0032-3861/99/$ - see front matter 
PII: S0032-3861(99)00063-4

compounds to study the higher order scattering reflections [6]. They concluded that bis(4-benzoyloxyphenyl) isophthalate is a good model for HIQ-*x*. HIQ-*x* has also been investigated using NMR by a number of groups. Gerard et al. [8,9] and Wiesner et al. [10] have investigated the local dynamics of various HIQ-*x* compositions in isotropic solutions and unoriented powders using $^{13}C$ NMR. They concluded that the ring mobility of the monomers is highly restricted and that decreasing the ring mobility correlates with higher sample crystallinities. Rutledge and Ward used solid-state $^{1}H$ NMR to study the orientation in HIQ-*x* on the molecular- scale [11]. Liao and Rutledge have used natural abundance, multi-dimensional, solid-state $^{13}C$ NMR techniques to investigate the orientation in HIQ-35 materials. They characterized the orientation distribution of the constituent monomers using a combination of anisotropic (Gaussian shaped) and isotropic functions [12].

RIS calculations [11,13] and structure factor calculations for arrays of extended chains [5,14–16] have also been employed to characterize the molecular conformation of HIQs. Simulation work on HIQ-*x* has focused primarily on the single chain and crystalline packing structures of the material. Johnson et al. determined chain conformations in HIQ-*x* in fibers by matching experimental WAXS peaks along the meridian with the calculated structure factors for single chains and planar arrays of chains [5,14–16]. They concluded that the chains of HIQ-*x* display planar zig-zag conformations comprised of rod-like sections joined by isophthalate ''hinges.'' This zig-zag formation is necessary for the proper extinctions to occur in the scattering pattern. Johnson et al. also suggested that the planarity of the chain conformations mitigates some of the modulus-degrading effects associated with the introduction of *m*-phenylene moieties. To model the conformational behavior of polyarylates, including HIQ-*x*, we have previously reported an RIS description for aromatic polyesters [13]. For compositions approaching $x = 100$ (i.e. poly(*p*-hydroxybenzoic acid)), the theoretical stiffness, persistence length, and shape anisotropy of the chains rise dramatically.

While considerable attention was given to describe single chain conformations and crystalline structure of HIQ-*x*, relatively little attention has been paid to the solid-state non-crystalline structure of these aromatic polyesters. Characterizing both the non-crystalline and crystalline structure of these polyarylates is necessary for a quantitative description of the molecular-scale structure and its relationship to macroscopic properties. For HIQ-*x*, this is particularly significant because the introduction of ''kinked'' *m*-phenylene moieties at random in the chain architecture leads to potentially large deviations from linearity of the chain backbone in these otherwise extended molecules. This non-linearity has important implications for packing correlation in the solid state and for the trade-off between tensile and compressive properties in fibers, films and injection molded materials.

Pole figure analysis is an established technique for measuring the orientation distribution of crystallites, and hence of their molecular constituents [17–20]. However, non-crystalline material is more problematic. Non-crystalline phases often account for more than half of the material in a processed semi-crystalline sample. Methods such as birefringence [21] and NMR [11,12] are effective for measuring the orientation of specific molecular constituents. However, these methods do not discriminate between crystalline and non-crystalline components as effectively as X-ray diffraction methods do, making their results somewhat more difficult to interpret in the case of semi-crystalline polymers. Except in special situations, these methods are also not very sensitive to the manner in which these molecular constituents are packed, i.e. the distance and orientation relationship between two constituents on the same or different molecules, in the solid state. Unlike X-ray scattering and NMR, birefringence measurements suffer from the additional limitation that they reveal only the first two moments of an orientation distribution, limiting their ability to provide the full orientation distribution function (ODF). In principle, X-ray diffraction can be used to study the structure and orientation of molecular level constituents in non-crystalline material, but the analysis is complicated by the fact that the observed scattering reflects contributions due to both intramolecular (conformational) and intermolecular (packing) disorder, in addition to misorientation of the basic structural units. In this paper, we explore the use of X-ray diffraction methods in combination with molecular simulations to identify a reasonable representation of the scattering unit, as an ensemble of scatterers, and its orientation in processed polymer solids.

Several previous investigations have used small angle and wide angle X-ray scattering to deduce structural information about non-crystalline material in polymers. Bartczak et al. and Galeski et al. [22,23] investigated uniaxially deformed specimens of both polyethylene and Nylon-6,6 processed in plane strain compression. They used pole figure diagrams to analyze the orientation in crystalline and non-crystalline portions of their samples and deduced the mechanical deformation mechanisms responsible for the development of orientation. For both polymers, deformed up to compression ratios of 6.44, they observed the development of a hexagonal arrangement of chains, like ''molecular cylinders'', in the non-crystalline material. Pieper and Killian [24] have also proposed a model wherein chain segments are treated as ''molecular cylinders'' which constitute the primary structural units of the non-crystalline solid. These structural units were then considered to arrange parallel to each other with varying degrees of lateral disorder to form cylindrically symmetric monodomains, which in turn constitute the macroscopic solid or melt. Murthy et al. [25,26] employed maximum entropy methods and modified Lorentzian peak shapes to deconvolute crystalline and non-crystalline WAXS scattering in a number of semi-crystalline polymers, such as poly(ethylene terephthalate), polyethylene, and Nylon-6,6. They characterized

the non-crystalline orientation in terms of an isotropic and an anisotropic portion. Fu et al. [27–29] deconvoluted the WAXS fiber patterns of PET fibers using a three component model and demonstrated the need for whole-pattern fitting for the crystalline portions of the pattern. They measured non-crystalline orientation in terms of a single parameter, $\langle P_2(\cos\phi)\rangle$, for the most intense non-crystalline feature only. Iannelli [30,31] studied semi-crystalline poly(aryl-ether-ether-ketone) and polyisobutylene with WAXS using a two-dimensional Rietveld analysis. In order to separate the crystalline and non-crystalline contributions, he assumed a Gaussian peak shape for the non-crystalline component. These studies reveal the value of information contained within both oriented and unoriented non-crystalline material, as well as highlight the problems associated with analyzing WAXS data for structure in poorly resolved patterns. In each case, however, the non-crystalline features of the pattern were characterized, and subsequently analyzed, using prescribed peak shapes.

Mitchell and co-workers [32–35] have developed a systematic approach for obtaining cylindrical distribution functions (of electron density) from WAXS of oriented, non-crystalline polymer, and from this the orientation distribution of chain segments. The cylindrical distribution function was conveniently expanded as a series of Legendre polynomials. The scattering observed from a distribution of independent structural units may be expressed as the convolution of the orientation distribution for the units with the scattering from a single unit [36]. Using this, and the assumption that chain segments could be treated as independent scatterers, Mitchell and Windle computed the theoretical structure factors for chain segments in various conformations. They then compared these with the observed scattering, at large scattering angles where interchain packing contributions are less important. From this comparison, they obtained an ODF for the chain segments. This approach was applied to poly(methyl methacrylate) [33,35] and to a liquid crystal copolymer composed of ethylene terephthalate and *p*-acetoxybenzoic acid [34]. Our approach employs a similar deconvolution of the scattering pattern into orientational and structural contributions. The identification of an ODF for a non-crystalline polymer depends critically on the identity and structure of the scattering unit, including interchain packing correlations. For this purpose, we devise a Monte Carlo simulation which samples the average scattering from an ensemble of molecular scale structural units. The simulation is constructed in a manner which selects units from an equilibrium ensemble such that the total calculated scattering function converges to the observed scattering.

This paper is organized as follows. In Section 2, we review the analysis of the WAXS fiber pattern in terms of cylindrical distribution functions, expressed as a series of Legendre polynomial terms. We then describe our model of the scattering unit in the solid state and the determination of both the structure and orientation distribution function for this scattering unit. In Section 4, we illustrate this approach with application to solution-spun fibers of HIQ-40. Finally, we discuss the implications of this analysis.

## 2. Methodology

### 2.1. Experimental data deconvolution

The analysis of oriented polymers by X-ray scattering methods is simplified by description in terms of angular coordinates. In general, the scattered intensity, $I(s,\alpha,\beta)$, is a function of the magnitude of the scattering vector, $s$, and the Euler angles, $\alpha$ and $\beta$ [37,38], relating its orientation to the frame of observation. Expansion of this general description in terms of suitable basis functions permits straightforward analysis. For the general case of scattering from an anisotropic sample, spherical harmonics have been suggested by Hobson [39] and frequently used [40–43]. For the purpose of the present analysis, involving samples exhibiting fiber symmetry, $I(s,\alpha)$ only, a simpler description using Legendre polynomials is adequate. Although of general utility in principle, the Legendre polynomial series expansion is most useful for smoothly varying functions with moderate degrees of orientation; higher degrees of orientation require determination of more terms and coefficients in the expansion, which can ultimately become problematic.

Fig. 1 illustrates the basic steps in the analysis presented here. This figure highlights the fact that a number of corrections to the experimental data are required before comparison to the model structure factor calculations. Fig. 1 summarizes the type of information needed to account for instrumental, geometrical, and structural features in the data. We used an amorphous reference, either simulated or experimental, to determine the geometrical and instrumental corrections to the experimental data. Using methods similar to those employed by Murthy et al. [25,26], the experimental data are then separated into crystalline and non-crystalline portions. The data are then renormalized, so that they may be compared to theoretical structure factor calculations. We describe the non-crystalline portion using the Legendre polynomial series expansion. Lastly, we introduce a molecular model with explicit atomic coordinates and calculate a theoretical structure factor. The theoretical structure factors are compared to those of experiment and, if the agreement of scattering features is reasonable, the model is accepted as a molecular level description for the material. As we are dealing with the non-crystalline portion of the WAXS pattern, we construct an *ensemble* of molecular scale structures to represent the system's oriented non-crystalline component. The relationship between the theoretical and experimental structure factor coefficients is quantified in the ODF.

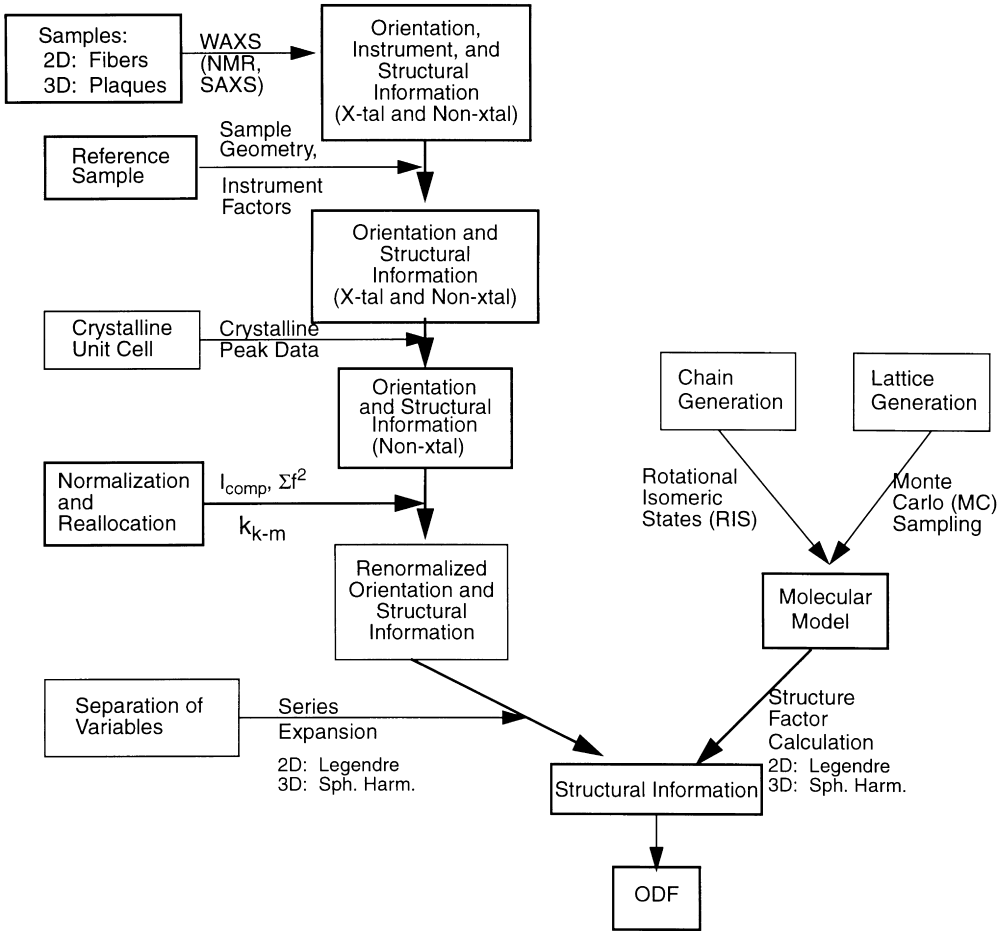


Fig. 1. Flowchart of the various steps, factors, and assumptions that enter the series expansion analysis. The left side lists the various parts of the data which are accounted for (instrumental, geometrical, crystalline, and theoretical) in the experimental data. The analysis culminates in a correlation of a molecular model to structural information derived via the series expansion.

The observed scattering intensity from the non-crystalline portion of an oriented polymer sample, $I_{ex,a}(s,\alpha)$, is separated into structural and orientational contributions, and the latter is expanded in terms of the basis functions:

$$I_{ex,a}(s,\alpha) = \sum_{n=0}^{\infty} A_{2n}(s)\, P_{2n}(\cos\alpha), \tag{1}$$

where the structure factor coefficient traces, $A_{2n}(s)$, are defined from the orthogonality of the basis functions as:

$$A_{2n}(s) = (4n+1)\int_0^{\pi/2} I_{ex}(s,\alpha)\cdot P_{2n}(\cos\alpha)\sin\alpha\, d\alpha \tag{2}$$

where $A_{2n}(s)$ are the functions of the scattering vector magnitude $s$, and therefore depend only on the structure of the scattering unit and not on its orientation. In Eqs (1) and (2), $\alpha$ is the azimuthal angle, measured with respect to the fiber axis in this case. $P_{2n}(\cos\alpha)$ are the Legendre polynomials of even order, $2n$, where $n = 0,1,2,\ldots$, and are used to construct the orientation distribution function, $D(\alpha)$. Due to symmetry, only even terms in the series contribute to the observed intensity and have been retained in Eq. (1). For semi-crystalline polymers in general, it is necessary to distinguish between the crystalline contribution, $I_{ex,x}(s,\alpha)$, and the non-crystalline contribution, $I_{ex,a}(s,\alpha)$, to the total observed scattering intensity. This is often possible using conventional methods of WAXS analysis to determine the contribution from crystalline material [17,18,25–31], and then taking the difference between the observed intensity and that attributed to crystallites to obtain $I_{ex,a}(s,\alpha)$. For the fibers analyzed here, the crystallinity as measured by WAXS is negligible, and accounting for this component of the scattering was not necessary.

Given a simple model for the independent structural unit responsible for X-ray scattering, one can compute a theoretical structure factor and the coefficient traces, $A_{2n}^{calc}(s)$. From the convolution of the theoretical structure factor coefficient with an orientation distribution function, $D(\alpha)$, to obtain the observed structure factor coefficient, one obtains the relation between two traces:

$$A_{2n}(s) = \frac{4n+1}{4\pi} D_{2n}\cdot A_{2n}^{calc}(s) \tag{3}$$

The scaling factors, $D_{2n}$, yield the coefficients in the basis set expansion for the orientation distribution function, $D(\alpha)$:

$$D(\alpha) = \sum_{n=0}^{\infty} \frac{4n+1}{4\pi} D_n \cdot P_{2n}(\cos\,\alpha) \tag{4}$$

where:

$$2\pi \int_0^{\pi} D(\alpha) \sin\,\alpha\, d\alpha = 1 \tag{5}$$

Note that the scaling factors relating the coefficient traces in Eq. (3) are scalars which affect the magnitude, but not the shape, of the calculated coefficient traces. A trace-by-trace comparison of $A_{2n}(s)$ with $A_{2n}^{calc}(s)$ provides a rapid, qualitative assessment of the validity of the model assumed in order to compute $A_{2n}^{calc}(s)$. Further, discrepancies observed in certain traces can offer guidance in how to refine the model. The construction of a suitable model, which is discussed in the next section, may involve only a simple conformational averaging of single chains, as was done by Mitchell and co-workers [33–35] or it may require intermolecular coordination statistics, such as that invoked by Pieper and Killian [24]. The better the agreement between the experimentally observed structure factor coefficient traces and their theoretically calculated counterparts, the more confidence one may place on the scaling factors, $D_{2n}$.

Up to this point, we have implied that two components may be needed to describe a polymer solid, crystal and non-crystal. In semi-crystalline polymers, there may be multiple crystal forms, or polymorphism, the presence of which may be deduced from the crystal diffraction pattern based on indexing of peaks. However, it is also possible that more than one type of structure exists in the non-crystalline phase as well, depending on how one chooses to model the non-crystalline component. As we assume that the oriented non-crystalline material exhibits local alignment of chains, we also allow for a second, isotropic non-crystalline material which is free of such local alignment. This unoriented material contributes only to the $A_0(s)$ term in the basis set expansion for scattered intensity. A priori, we do not know the relative contribution of the unoriented non-crystalline phase to the $A_0(s)$ trace; however, it is not assumed to be negligible.

### 2.2. Molecular model of scattering unit

The scattering unit for an oriented, non-crystalline component should consist of an ensemble of anisotropic units. Previous workers have assumed the smallest representation of independent scatterers to be the chains themselves [33]. There, the ensembles consisted of short sections of a chain of representative composition, usually in a statistically-weighted set of conformations as determined by equilibrium considerations, such as in rotational isomeric state (RIS) modeling. By considering only short sections of chains, and performing the ensemble average over statistically independent, but completely aligned, segment conformations (e.g. parallel end-to-end vectors), the chain segment scattering unit retains anisotropic character. In this work, we wish to explore the effect of packing correlation between chains and deviations of the single chain conformation distribution from its ideal (e.g. $\theta$-state) distribution due to the effects of packing with other chains. For this purpose, we construct small, atomistically-detailed structures consisting of segments of several chains with several monomers per segment. We rely on a Monte Carlo scheme to sample the appropriate distribution of such structures in a manner which is both consistent with packing constraints, and yet reproduces the observed scattering behavior.

To construct our molecular model, we first build sections of the polymer chain with conformations according to their single chain statistics. Consistent with previous work, we have employed an RIS description (i.e. chains have fixed bond lengths, fixed bond angles and discrete isomeric torsion states for each bond) for the chain conformations. An RIS parameterization for aromatic copolyesters of various compositions has been reported previously [13] and is used here for HIQ-*x*. In this model, the aromatic rings are treated as rigid moieties. The ester group is believed to exist predominantly in the planar *trans* state. However, estimates of persistence lengths for numerous polyarylates indicate that a single *trans* state for this bond tends to overestimate the rigidity of the chain [13]. For this reason, the ester torsion was allowed to take values between $\pm$ 30° from *trans* with equal probability. Rotation about a ring-carbonyl carbon bond may be either *cis* or *trans* (carbonyl coplanar with ring). Rotation about a ring-ester oxygen bond may take any one of the four isomeric states ( $\pm$ 45°, $\pm$ 135°) with equal probability, each rotating the ester group 45° out of the plane of the neighboring aromatic ring. These angles were derived from single chain quantum chemistry calculations; experimental data and Monte Carlo simulations on copolyesters in the solid state suggest that these angles are usually closer to 60°–70° out of plane [44] due to thermal motion and packing interactions [45]. However, this correction was not taken into account here. The persistence length for HIQ-*x* in the range $30 < x < 50$ was estimated to vary from six to eight monomers (33-44 Å) in length. On a length scale shorter than this, the molecular segments are highly anisotropic and may be aligned; as described previously [11], we computed the radius of gyration tensor for each generated conformation, and then averaged the conformations with the major axis of this tensor parallel for all conformations. Up to this point, our single chain model for the scattering unit is comparable to those described earlier.

To evaluate the role of interchain packing on the scattering unit, we not only consider the isolated chain segments, but also the collections of segments packed together on a 2D lattice lateral to the alignment direction. Chain segments of different conformations are generated according to their Boltzmann-weighted probability within the RIS approximation and placed on each site of the 2D lattice with their

centers of mass on the lattice points. The major axis of the radius of gyration is aligned parallel to the unique axis of the model and the chain is rotated by a random setting angle about its alignment axis. The lattice itself is expected to be close to hexagonal [19,20,22,24,46], but the three parameters required to define the lattice periodicity (two lattice distances, $a$ and $b$, and the angle $\gamma$ between them) were varied from model to model. Statistical distortions of the lattice, such as Hosemann's paracrystallinity, were considered only approximately, as follows. Each chain was placed on the lattice with displacement of its center of mass from the lattice site taken from uniform distributions between $\pm \Delta a$ and $\pm \Delta b$. For lattice sites beyond the cut-off of the lattice size, the segments are assumed to be completely uncorrelated with the lattice, making no contribution to the structure factor of the scattering unit. The primary effect of the local distortions is to attenuate intensity in the peaks, as in Type I paracrystallinity [47,48]. Truncation of the lattice serves as a crude approximation to the gradual loss of correlation described by Type II paracrystallinity and similar types of lattice statistics. By varying the number of chain segments, the number of monomers per segment, the spacing and angle between chains on the lattice, and distortions about the local lattice positions, we explore different models for the scattering unit in the presence of interchain packing interactions.

In order for Eq. (3) to hold, the structure factor $A_{2n}^{\text{calc}}(s)$ of the scattering unit must be cylindrically symmetric and was computed using the following equation [17,40,41]:

$$A_{2n}^{\text{calc}}(s) = \frac{4n+1}{N} \sum_{j}^{N} \sum_{k>j}^{N} f_j(s)\, f_k(s)\, J_{2n}(r_{jk}s)\, P_{2n}(\cos\alpha_{jk}) \tag{6}$$

where the double summation runs over all pairs of atoms in the current structure, $f_j(s)$ and $f_k(s)$ are the atomic scattering factors for atoms $j$ and $k$, respectively, $J_{2n}(r_{jk}s)$ is the Bessel function of order $2n$, $r_{jk}$ is the distance between atoms $j$ and $k$ and $\alpha_{jk}$ is the angle between the vector connecting atoms $j$ and $k$ and the axis of alignment. It is important to recognize that the scattering unit of the non-crystalline component is not a single structure, but rather an average over an ensemble of structures. Our ensemble consists of structures derived from the configuration space defined by the aforementioned model construction. In order to sample the ensemble, we employ a simple Metropolis Monte Carlo algorithm. The energy, $E_{\text{new}}$, of each newly generated structure is calculated and the structure is accepted or rejected according to the standard Metropolis criterion:

$$p = \min(1, \exp(-\beta_T(E_{\text{new}} - E_{\text{old}}))) \tag{7}$$

where $\beta_T$ is $1/k_B T$. As the individual chain conformations are generated according to their proper statistical probabilities from the RIS parameterization, only the interchain energy is included in the Metropolis criterion. In this work, we have used a simple hard-core potential for interatomic interactions between chain segments. Structures in which atoms $j$ and $k$ on different segments are separated by less than the sum of their hard core radii, $d_{jk} < (d_{\text{vdw},j} + d_{\text{vdw},k})/2$, are rejected, ($E_{\text{new}} = \infty$), while those without any such overlaps are accepted, ($E_{\text{new}} = 0$). In this way, structures involving unfavorable packing interactions are eliminated from the structure factor average of the scattering unit. With the crude interatomic potential used here, the inverse temperature of the simulation, $\beta_T$, may take any non-zero value.

Due to the influence of processing, the ensemble of structures comprising the non-crystalline component may not be representative of the equilibrium distribution described by Boltzmann weights. We have no way to know a priori to what extent the distribution of states is distorted from equilibrium. To reflect this distortion, we modify the Metropolis criterion to bias acceptance in favor of structures which improve the agreement between the theoretical and observed structure factors:

$$p = \min(1, \exp(-\beta_T(E_{\text{new}} - E_{\text{old}}))\cdot\exp(-\beta_\chi(\chi^2_{\text{new}} - \chi^2_{\text{old}}))) \tag{8}$$

where $\chi_i^2$ is the sum of squared deviations between the theoretical and experimental structure factors computed at sample $i$. It serves a role analogous to a thermodynamic energy in the Monte Carlo sampling, but it is not of thermodynamic origin. It provides a ''measure of merit'' by which the distribution of states sampled in the simulation is biased to obtain better correspondence between the model and experimental structure factors. Such biasing is necessary in order to compensate for the effects of processing history, which alter the distribution of microstates from that expected in the absence of such memory. $\chi_i^2$ is computed as follows:

$$\chi_i^2 = \frac{1}{iN'} \sum_{k=1}^{i} \sum_{n=0}^{N'} \int_{s_0}^{s_f} (A_{2n}(s) - D'_{2n,i}\, A_{2n,k}^{\text{calc}}(s))^2\, \mathrm{d}s \tag{9a}$$

$$\chi_i^2 = \frac{1}{N'} \sum_{n=0}^{N'} \int_{s_0}^{s_f} \langle(\Delta A_{2n}(s))^2\rangle_i\, \mathrm{d}s \tag{9b}$$

where $s_0$ and $s_f$ are the limits of available data; $N'$ indexes the highest term retained in the truncated series expansion. In order to compute $\chi_i^2$ by this equation, the theoretical structure factor coefficient traces must be scaled for comparison. At each step, the $D'_{2n}$'s are chosen such that they minimize $\chi_i^2$ for the total ensemble, hence giving the highest probability for acceptance. $\beta_\chi$ is a weighting factor which moderates the influence of the bias function in $\chi_i^2$. It is analogous to an inverse ''temperature''. For $\beta_\chi$ equal to zero, the simulation reverts to the standard Metropolis Monte Carlo with Boltzmann statistics. As the value of $\beta_\chi$ is increased, the simulation becomes more like a numerical refinement technique, wherein only those structures which improve the global fit of the simulation to the observed data

Table 1
The van der Waals radii for the various atom types in our simulations. $C_{ph}$ is a phenylene ring carbon, C*, a carbonyl carbon, O′, a carbonyl oxygen, O, an ether oxygen, and H, a hydrogen

| Atom type | $C_{ph}$ | C* | O′ | O | H |
|---|---|---|---|---|---|
| $d_{vdw}$ (Å) | 1.96 | 2.03 | 1.60 | 1.60 | 1.37 |

are retained. A reasonable upper bound for $\beta_\chi$ may be related to the statistical error of the experimental data which the model attempts to describe, e.g. $\beta_\chi = 1/2\sigma^2$ if the error is assumed to be normally distributed with standard deviation $\sigma$. Intermediate values of $\beta_\chi$ may be chosen to adjust the weight of the experimental data relative to the energy calculation in the ensemble sampling. It should be noted that, in contrast to the usual Markov chain used in Monte Carlo simulations, the bias function implemented here depends on all previously accepted states $k < i$ in the simulation, an $i$-th order Markov process. This was chosen because the observation on which the bias function is based, the structure factor, is itself a distribution which reflects the contributions from all the elements of the ensemble. Thus, $\chi_i^2$ is path-dependent and a property of the entire simulation rather than of a particular member of the ensemble.

## 3. Analysis of HIQ-40 fibers

### 3.1. Experimental

The method described in the previous section is demonstrated by the application to a sample of HIQ-40 fibers spun from an isotropic solution of 20% dichloromethane and 80% trifluoroacetic acid. The fibers were provided by Hoechst–Celanese (Summit, New Jersey) and are analyzed ''as-spun'' without any post-processing heat treatment. The fibers are 42.6 ± 0.6 μm in diameter as measured by optical microscopy. The experimental WAXS fiber pattern was collected using a Rigaku RU200B rotating copper anode. The wavelength of radiation for the CuK$\alpha$ emission is 1.54 Å. Scattering data were taken over an angular range of $2\theta = 10°$–$50°$ in steps ($\Delta 2\theta$) of 0.1°. A pole figure attachment on the $\theta/2\theta$ goniometer allowed us to take sixteen $\theta/2\theta$ traces over the entire azimuthal angular range, $\alpha = 0°$–$90°$ with $\Delta\alpha = 6°$.

The raw data were normalized to atomic units (a.u.), a measure of the theoretical scattering power of the material on a per atom basis, using the method reported by Krogh–Moe [49], also employed by Mitchell and Windle [33,35]. The normalization factor, $k_{k\text{-}m}$, was determined using the following relation:

$$k_{k\text{-}m} = \frac{\int_{s_0}^{s_f} s^2\, I'(s)\, \mathrm{d}s - 2\pi^2 Z\rho}{\int_{s_0}^{s_f}\int_0^{(\pi/2)} s^2\, I_{raw}(s,\alpha)\sin\alpha\, \mathrm{d}\alpha\, \mathrm{d}s} \tag{10}$$

The numerator represents the integrated intensity of the total uncorrelated scattering, $I'(s)$, which comprises both the coherent self-scatter, $\Sigma f^2(s)$, and the incoherent Compton scatter, $I_{comp}(s)$, of all the atoms in the specimen. $I'(s)$ is a function of sample composition only, and was computed using standard relations [50]. From the integral of $I'(s)$, we subtract the zero-angle scattering intensity; $Z$ is the total electron charge and $\rho$, the atomic density of the material. The denominator of Eq. (10) is the total integrated intensity of the experimentally observed scattering, $I_{raw}(s,\alpha)$. The experimental data were then multiplied by $k_{k\text{-}m}$ to express the intensity in a.u., from which the electron gas and Compton scattering were subtracted to obtain $I_{ex}(s,\alpha)$, an interference function which represents the deviation of the scattering function from that of the homogeneous electron gas:

$$I_{ex,a}(s,\alpha) = k_{k\text{-}m} I_{raw}(s,\alpha) - I_{comp}(s) - \sum f^2(s) \tag{11a}$$

$$I_{ex,a}(s,\alpha) = k_{k\text{-}m} I_{raw}(s,\alpha) - I'(s) \tag{11b}$$

where $I_{ex,a}(s,\alpha)$, the adjusted experimental intensity, contains both positive and negative regions as it represents a re-allocation of scattered intensity about a mean (the uncorrelated scattering), due to the presence of atomic-level structure. This interference function was then deconvoluted into a series of Legendre polynomial terms and their corresponding structure factor coefficient traces, as described in Section 2. The noise level in the data ultimately places an upper bound on the number of terms which may reasonably be evaluated; we chose to extend the series until the square root of the sum of squared deviations between the calculated and experimental patterns was less than 10% of the total integrated intensity of the pattern.

For the determination of $A_{2n}^{calc}(s)$, the model consisted of $N_l^2$ chain segments, each $m$ units long place on an $N_l \times N_l$ lattice. We considered lattices with up to 25 chains, each chain being up to 15 monomers long. Monomers were chosen at random to construct each chain segment, subject to the constraints that only appropriate ester linkages between monomers were formed and that the overall sampled composition of structures in the model was 40% 1,4-hydroxybenzoate, 30% isophthalate and 30% hydroquinone. The conformation of each segment was selected according to the RIS model described previously [13]. Lattice distances, $a$ and $b$, were tested between values of 3.0 and 6.0 Å with 0.25 Å steps. The local displacements of the chains about the average lattice positions were allowed to vary uniformly up to ± 50% of the lattice spacing itself (i.e. $\Delta a = a/2$, $\Delta b = b/2$). The result is a fairly disordered ''lattice''. The lattice angle, $\gamma$, was tested over values of 60–90° with 10° steps. van der Waals radii for each atom type used in the model were obtained from the cvff force-field [51] and are shown in Table 1. The critical overlap distance was taken to be a fraction of the sum of van der Waals radii, $d_{jk} < K_{vdw}\cdot(d_{vdw,j} + d_{vdw,k})/2$, where $K_{vdw} = 0.5$

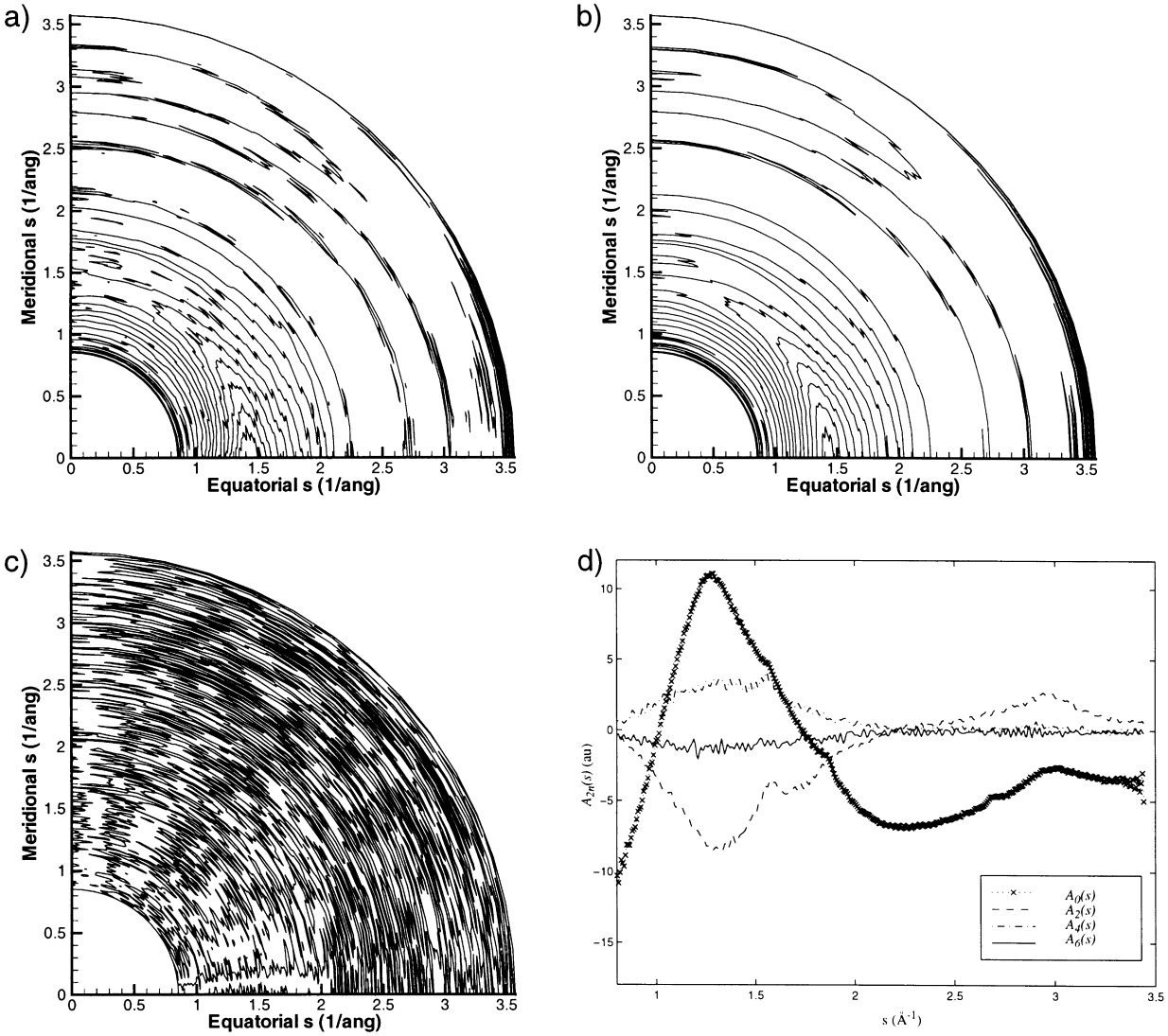


Fig. 2. Reconstruction of HIQ-40, as-spun, solution spun fiber. (a) raw data, 16 contours; (b) reconstructed data from the Legendre polynomial series expansion, 16 contours; (c) difference spectrum, 3 contours; (d) experimental coefficient traces, $A_{2n}(s)$ for $2n = 0$–6. All contour plots have two counts/contour.

was used in most cases. The weight factor, $\beta_\chi$, used here was $1.2 \times 10^{-3}$. Thus, the distribution sampled should be close to the thermodynamic one, and only weakly biased to match the data. Due to the length of calculation of structure factors at each step, the simulations were short by Monte Carlo standards, typically between $0.5 \times 10^4$ and $1 \times 10^4$ structures, with acceptance rates of the order of 10%.

### 3.2. Results and discussion

The results of the experimental data analysis for the HIQ-40 solution-spun fibers are illustrated in Fig. 2. $I_{ex,a}(s,\alpha)$ ($= I_{ex}(s,\alpha)$ for these fibers) obtained from Eqs. (11a) and (11b) is shown in Fig. 2(a). A series expansion in Legendre polynomials up to order $n = 3$ was found adequate to represent $I_{ex,a}(s,\alpha)$ according to Eq. (1) and is shown in Fig. 2(b). Fig. 2(c) shows the difference pattern between the original and reconstructed experimental interference patterns, which is essentially featureless, and Fig. 2(d) shows the individual structure factor coefficient traces, $A_{2n}(s)$, up to $n = 3$. The relatively rapid convergence of the series confirms the low level of orientation in these fibers.

Three features located at 20.3°, 27.1° and 44.6° in $2\theta$ ($s =$ 1.436, 1.909 and 3.091 Å$^{-1}$, respectively) are consistent from trace to trace (Table 2). The presence of these three features in the higher order ($n > 0$) traces indicates that these must be characteristic of the scattering unit present in

Table 2
Summary of spacings in experimental coefficient traces for HIQ-40 as-spun, solution-spun fibers

| | $2\theta$(°) | $d$ (Å) | $s$ (Å$^{-1}$) |
|---|---|---|---|
| Peak 1 | 20.3 | 4.375 | 1.436 |
| Peak 2 | 27.1 | 3.291 | 1.909 |
| Peak 3 | 44.6 | 2.033 | 3.091 |

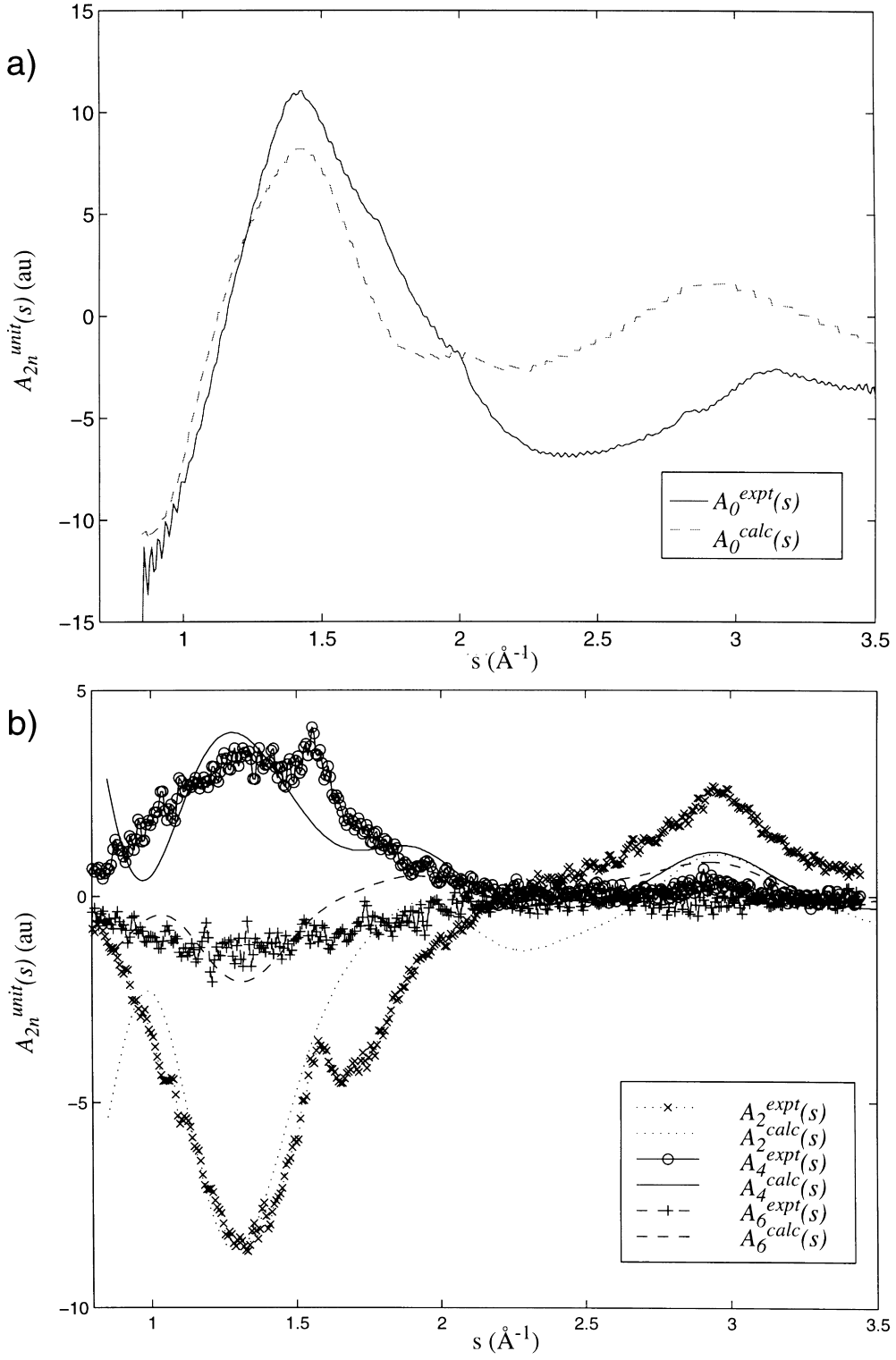


Fig. 3. Comparison of experimental and calculated structure factor coefficient traces for HIQ-40 as-spun, solution-spun fibers, (a) $A_0(s)$ coefficients, (b) $A_{2n}(s)$ coefficients ($2n = 2,4,$and 6)

the oriented, non-crystalline component of the polymer. They were used to reject models wherein these features were either shifted or of different breadth from the experimental observations. Using the molecular model and searching the parameter ranges outlined before, the peak at $s = 3.091$ Å$^{-1}$ was found to be an intrachain scattering feature and most sensitive to conformational characteristics of the RIS model. By varying the length and flexibility of

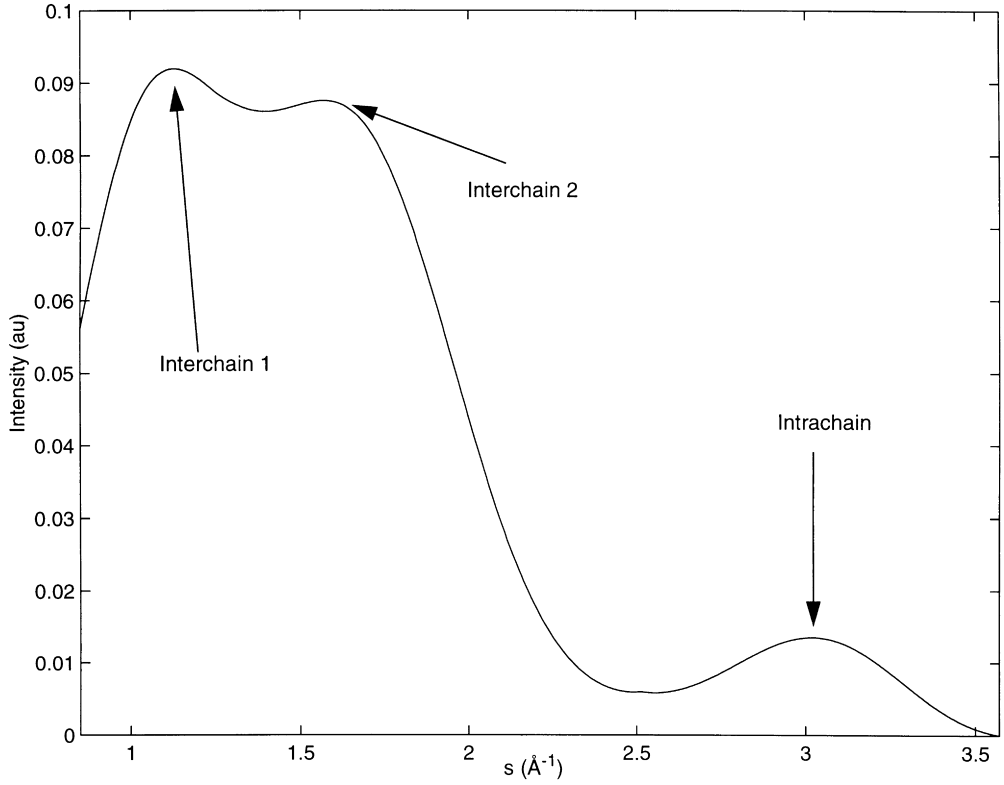


Fig. 4. Simulated amorphous structure factor calculation for HIQ-40 from Biosym[tm].

the chain segments, this peak could be reproduced in each trace. The peaks at $s = 1.436$ and 1.909 Å$^{-1}$ are predominantly interchain scattering features and were reproduced by varying the number of chains and parameters of the lattice. The best overall results were obtained with a model consisting of dimer segments on a $3 \times 3$ lattice with $a = 4.25$ Å, $b = 3.75$ Å, and $\gamma = 80°$. This model yielded theoretical coefficient traces with the proper features observed in the experimental data out to the $A_6(s)$ term. Using Eq. (3), the higher order scaling coefficients, $D_{2n}$, ($n > 0$) were determined by minimizing the sum of squared deviations between the observed trace and the scaled model trace. The agreement between the observed and calculated traces for $A_2(s)$, $A_4(s)$, and $A_6(s)$ are shown in Fig. 3(b). The divergence of the $A_{2n}^{calc}(s)$ curves as $s$ approaches zero is an artifact of the small size of the model cluster of chains.

After identifying a suitable model to describe the higher order coefficient traces, we found that the isotropic coefficient trace, $A_0(s)$, was still not adequately reproduced in terms of relative heights and breadths of the three main features. To compensate for this shortcoming, we concluded that a second, isotropic scattering component must be present in the fibers, whose structure does not possess local alignment of chain segments. This isotropic material was modeled using conventional molecular simulations. A cubic, amorphous cell with sides measuring 20.96 Å was packed with 50-mer chains of HIQ-40 to a density of 1.35 g/cm$^3$ [52]. The amorphous cell was constructed using the polymer modules of Biosym/MSI [51]. This was followed by NVT molecular dynamics simulations using Discover v3.2$\beta$ with the cvff force field at 300 K. Temperature control was maintained using velocity rescaling. The system was allowed to equilibrate for 50 ps using 1 fs steps and 10 snapshots of the system were then collected at 100 ps intervals. The structure factor for the isotropic component of HIQ-40 was then computed from the average over these 10 structures and is shown in Fig. 4. Interestingly, this simulation also shows three features similar to those observed experimentally and in the model of the non-crystalline component, but with different relative intensities and no orientation dependence.

Finally, the $A_0(s)$ trace was fitted using the $A_0^{calc}(s)$ trace determined from the model of the oriented non-crystalline component and the structure factor for the isotropic non-crystalline component (Fig. 3(a)). Both the fractions of the oriented non-crystalline material, $X_{ONC}$, and the zeroth order scaling factor, $D_0$, for the oriented non-crystalline component were varied in order to minimize the sum of squared deviations between the two-component model trace and the

Table 3
Scaling coefficients, $D_{2n}$; $\chi^2_{2n}$ for HIQ-40 as-spun, solution-spun fibers

| 2n | 0 | 2 | 4 | 6 |
|---|---|---|---|---|
| $D_{2n}$ | 1 | 0.02 | 0.003 | 0.001 |
| $\chi^2_{2n}$ | 4.88 | 4.09 | 2.06 | 1.22 |

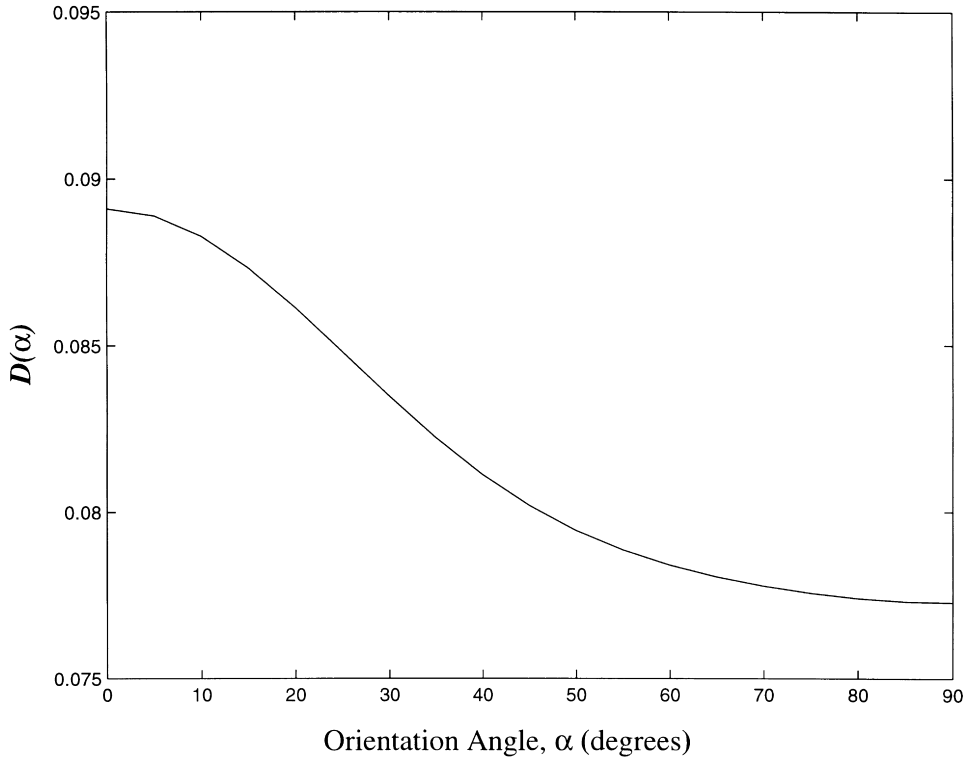


Fig. 5. ODF for HIQ-40, as-spun, solution-spun fibers.

observed experimental trace. The results for $X_{ONC}$ and $D_0$ and the scaling factors determined directly for the higher order contributions are shown in Table 3, along with the sum of squared deviations, $\chi^2_{2n}$, for each coefficient trace. For each trace, $\chi^2_{2n}$ is about an order of magnitude smaller than the maximum value of $(A_{2n}(s))^2$. From the values of $D_{2n}$, the orientation distribution function, $D(\alpha)$, for the anisotropic non-crystalline component is reconstructed and is shown in Fig. 5. The anisotropic portion of the distribution has a FWHM of 64.6° and is only weakly oriented. However, the oriented non-crystalline component accounts for over 85% of the scattering. This implies that the chains in these HIQ-40 fibers exhibit strong local alignment, but that the global orientation of structures over the entire fiber is small.

The results reported here suggest that the size of the oriented non-crystalline domains required to describe independent scattering units is small. While some portion of the non-crystalline phase must be aligned with its neighbors locally in order to observe anisotropic scattering in the interchain features, this local alignment may be very short-ranged, e.g. nearest neighbors only. Further, the presence of a second, isotropic component suggests that a significant fraction of the material (about 15%) in these as-spun fibers is not even aligned locally. Although we have treated these two as separate components for the purposes of averaging, the very small correlation distances suggests that these two may be very intimately mixed; the two-component description is a matter of convenience only and is not intended to imply two distinct thermodynamic phases within the sample.

The series expansion analysis is most suited for describing samples with orientation which requires a few terms in the expansion. These are generally low levels of orientation. While, in theory, we can study any axisymmetric distribution and break it down in terms of a Legendre polynomial series expansion, very narrow distributions (i.e. high molecular orientations) require a large number of terms. For highly anisotropic systems, such as some products formed in industrial fiber processes, one can find that the number of coefficient traces necessary for a proper description of the orientation can be large. In these cases, the series expansion is limited in accuracy by the resolution of the experimental data in the azimuthal direction.

## 4. Conclusions

We have demonstrated the applicability of the series expansion analysis to the determination of an ODF and its associated structural ensemble for characterizing the non-crystalline component of an axisymmetric fiber sample of an aromatic polyester. The series expansion requires four terms (up to $n = 3$) for adequate characterization. The structural ensemble deduced from our simulations consisted of dimers placed on a $3 \times 3$ rhombic lattice. For the aromatic polyester used in the example, we invoke a two-component system to account for the features in the experimental WAXS results.

The two components are oriented and unoriented non-crystalline phases of the material. The analysis shows that the sample contains no detectable crystalline phase, but displays over 85% locally-aligned material.

We have also demonstrated the applicability of the series expansion analysis and our general data analysis methodology to both conformational and packing behavior in engineering materials. The conceptual advantages of the analysis are: (i) rigorous definition of the orientation distribution function, (ii) a quantitative correlation between theoretical calculation and experiment, (iii) an explicit interpretation of the structural ensemble, which may be subjected to further characterization and analysis for properties, and (iv) the reduced computational load required for the full pattern analysis, due to the reduction of the full 2D pattern into a smaller number of one-dimensional coefficient traces. We have presented a general methodology, which may easily be extended to other polymeric systems for orientational analysis under varying processing conditions. In the companion paper to this one, we apply this analysis to a set of polyarylate fibers generated by different processes. Straightforward extensions of the concepts presented here permit analysis of other polymers and other sample symmetries.

## Acknowledgements

The authors are grateful to Dr. S.H. Foulger for his help in conducting the Biosym/MSI calculations and for other helpful discussions, and to Dr. M. Jaffe for providing the fiber samples. Financial support for this work was provided by the National Science Foundation, award #CTS-9457111.

## References

[1] Blundell DJ, MacDonald WA, Chivers RA. High Performance Polymers 1989;1:97.
[2] Erdemir AB, Johnson DJ, Tomka JG. Polymer 1986;27:441.
[3] MacDonald WA, McLenaghan ADW, Richards HW. Macromolecules 1992;25:826.
[4] Blundell DJ, Chivers RA, Curson AD, Love JC, MacDonald WA. Polymer 1988;29:1459.
[5] Erdemir AB, Johnson DJ, Karacan I, Tomka JG. Polymer 1988;29:597.
[6] O'Mahoney CA, Williams DJ, Colquhoun HM, Blundell DJ. Polymer 1990;31:1603.
[7] Cao J, Karacan I, Tomka JG. Polymer 1995;36:2133.
[8] Gerard A, Laupretre F, Monnerie L. Macromolecules 1993;26:3313.
[9] Gerard A, Laupretre F, Monnerie L. Polymer 1995;19:3661.
[10] Wiesner U, Laupretre F, Monnerie L. Macromolecules 1994;27:3632.
[11] Rutledge GC, Ward IM. J Polym Sci Pol Phys 1993;31:513.
[12] Liao M-Y, Rutledge GC. Macromolecules 1997;30:7546.
[13] Rutledge GC. Macromolecules 1992;25:3984.
[14] Johnson DJ, Karacan I, Tomka JG. Polymer 1990;31:8.
[15] Johnson DJ, Karacan I, Tomka JG. J Text Inst 1990;81:421.
[16] Johnson DJ, Karacan I, Tomka JG. Polymer 1992;33:983.
[17] Guinier A. X-ray diffraction in crystals, imperfect crystals and amorphous bodies. New York: Dover Publishing, 1963.
[18] Alexander L. X-ray diffraction methods in polymer science. New York: Wiley Interscience, 1969.
[19] Galeski A, Argon AS, Cohen RE. Macromolecules 1991;24:3945.
[20] Bartzcak Z, Cohen RE, Argon AS. Macromolecules 1992;25:4672.
[21] Hamza AA, Fouda IM, El-Farahaty KA, El-Tonsy MM. Polymer Communications 1989;30:186.
[22] Bartzcak Z, Argon AS, Cohen RE. Macromolecules 1992;25:5036.
[23] Galeski A, Argon AS, Cohen RE. Macromolecules 1988;21:2761.
[24] Pieper T, Killian H-G. In: Zachmann HG, editor. Structure in polymers with special properties, Berlin: Springer, 1993, p. 4989.
[25] Murthy NS, Minor H, Bednarczyk C, Krimm S. Macromolecules 1993;26:1712.
[26] Murthy NS, Zero K, Minor H. Macromolecules 1994;27:1484.
[27] Fu Y, Busing WR, Jin Y, Affholter KA, Wunderlich B. Macromolecules 1993;26:2187.
[28] Fu Y, Annis B, Boller A, Jin Y, Wunderlich B. J Polym Sci Pol Phys 1994;32:2289.
[29] Fu Y, Busing W, Jin Y, Affholter KA, Wunderlich B. Macromol Chem Phys 1994;195:803.
[30] Iannelli P. Macromolecules 1993;26:2303.
[31] Iannelli P. Macromolecules 1993;26:2309.
[32] Mitchell GR, Lovell R. Acta Cryst 1981;A37:189.
[33] Mitchell GR, Windle AH. Colloid and Polymer Sci 1982;260:754.
[34] Mitchell GR, Windle AH. Polymer 1982;23:1269.
[35] Mitchell GR, Windle AH. Colloid and Polymer Sci 1985;263:230.
[36] Deas HD. Acta Cryst. 1952;5:542.
[37] Rose ME. Elementary theory of angular momentum. New York: Dover Publishing, 1954.
[38] Prince E. Mathematical techniques in crystallography and material science. New York: Springer, 1994.
[39] Hobson EW. The theory of spherical and ellipsoidal harmonics. New York: Chelsea Publishing, 1965.
[40] de Gennes PG. CR Acad Sc (Paris) 1972;274:142.
[41] Pynn RJ. Phys Chem Solids 1973;34:735.
[42] Sears VF. Can J Phys 1966;44:1279.
[43] Sears VF. Can J Phys 1966;44:1299.
[44] Blackwell J, Lieser G, Gutierrez G. Macromolecules 1983;16:1418.
[45] Foulger SH, Rutledge GC. J Polym Sci Pol Phys 1998;36:727.
[46] Galeski A, Argon AS, Cohen RE. Macromolecules 1991;24:3953.
[47] Hosemann R. Zs. Phys. 1950;128:1.
[48] Hosemann R. Direct Analysis of Diffraction by Matter. Amsterdam: Interscience Publishers, 1962.
[49] Krogh-Moe J. Acta Cryst 1956;9:951.
[50] Henry NFM, Lonsdale K. International Tables for X-ray crystallography. In: Henry NFM, Lonsdale KL, editors. Birmingham: The Kynoch Press, 1969, vol. 1, p. 16.
[51] Biosym[tm] version 2.3.6, available through Molecular Simulations Inc., 9685 Scranton Road, San Diego, CA 92121, 1994.
[52] Hsiao BS, Shaw MT, Samulski ET. J Polym Sci Pol Phys 1990;28:189.